Journal of the Association of Arab Universities for Basic and Applied Sciences (2016) **xxx**, xxx–xxx

University of Bahrain
Journal of the Association of Arab Universities for Basic and Applied Sciences
www.elsevier.com/locate/jaaubas
www.sciencedirect.com

Unsteady three-dimensional MHD flow of a nano Eyring-Powell fluid past a convectively heated stretching sheet in the presence of thermal radiation, viscous dissipation and Joule heating

B. Mahanthesh [a,b], B.J. Gireesha [b,c,*], Rama Subba Reddy Gorla [c]

[a] *Department of Mathematics and Statistics, Christ University, Bangalore 29, Karnataka, India*
[b] *Department of Studies and Research in Mathematics, Kuvempu University, Shankaraghatta 577 451, Shimoga, Karnataka, India*
[c] *Department of Mechanical Engineering, Cleveland State University, Cleveland 44114, OH, USA*

Received 29 June 2015; revised 20 May 2016; accepted 23 May 2016

KEYWORDS

Eyring-Powell fluid;
Joule heating;
Convective boundary condition;
Brownian motion;
Viscous dissipation;
Nanofluid

Abstract The purpose of this study is to investigate the unsteady magnetohydrodynamic three-dimensional flow induced by a stretching surface. An incompressible electrically conducting Eyring-Powell fluid fills the convectively heated stretching surface in the presence of nanoparticles. The effects of thermal radiation, viscous dissipation and Joule heating are accounted in heat transfer equation. The model used for the nanofluid includes the effects of Brownian motion and thermophoresis. The highly nonlinear partial differential equations are reduced to ordinary differential equations with the help of similarity method. The reduced complicated two-point boundary value problem is treated numerically using Runge–Kutta–Fehlberg 45 method with shooting technique. A comparison of the obtained numerical results with existing results in a limiting sense is also presented. At the end, the effects of influential parameters on velocity, temperature and nanoparticles concentration fields are also discussed comprehensively. Further, the physical quantities of engineering interest such as the Nusselt number and Sherwood number are also calculated.

1. Introduction

A boundary layer flow, heat and mass transfer over a stretching surface is a topic of great interest to the researchers in view of their engineering and industrial applications. Few applications are, metal and polymer extrusion, paper, glass and fiber production, wire drawing, metal spinning, drawing of plastic films etc. In these processes the final product is significantly depends on heat transfer rate. In addition, magnetohydrodynamics of

* Corresponding author at: Department of Mechanical Engineering, Cleveland State University, Cleveland 44114, OH, USA.
E-mail addresses: mahanthesh.b@christuniversity.in (B. Mahanthesh), g.bijjanaljayanna@csuohio.edu (B.J. Gireesha), r.gorla@csuohio.edu (R.S.R. Gorla).
Peer review under responsibility of University of Bahrain.

http://dx.doi.org/10.1016/j.jaubas.2016.05.004
1815-3852 © 2016 University of Bahrain. Production and hosting by Elsevier B.V.

Please cite this article in press as: Mahanthesh, B. et al., Unsteady three-dimensional MHD flow of a nano Eyring-Powell fluid past a convectively heated stretching sheet in the presence of thermal radiation, viscous dissipation and Joule heating. Journal of the Association of Arab Universities for Basic and Applied Sciences (2016), http://dx.doi.org/10.1016/j.jaubas.2016.05.004

an electrically conducting fluid is also important as it finds applications in various stretching sheet problems. For example in metallurgical processes, the magnetic field effect has a pivotal role. By drawing strips in MHD fluid, the rate of cooling can be controlled and the desired quality of end product can be achieved. Boundary layer flow of viscous fluid bounded by a moving surface was first studied by Sakiadis (1961). After the pioneering work of Sakiadis (1961), several attempts (Crane, 1970; Grubka and Bobba, 1985; Ishak et al., 2009) have been made on this topic.

On the other hand, several industrial fluids such as polymer solutions shampoos, paints, granular suspension, paper pulp, slurries, drilling mud's and certain oils are of the non-Newtonian fluid nature. The non-Newtonian boundary layer flow induced due to stretching of sheet has tremendous applications in many industrial and manufacturing processes. Thus researchers have shown their attention to study different non-Newtonian fluid models under different physical situations. For instance, Hayat et al. (2012a) Hayat et al. (2012b) presented the simultaneous effects of heat and mass transfer on flow of third grade fluid between two heated porous sheets. They employed similarity technique and Homotopy analysis method to obtain the analytical solutions. A steady Poiseuille flow and heat transfer of couple stress fluids between two parallel inclined plates with variable viscosity is presented by Farooq et al. (2013). An exact similarity solution is presented by Gorla et al. (1995) for steady three dimensional flow of power law fluid motion caused by stretching of the flat boundary in the lateral directions. They found that, pseudo plastic fluids display drag reduction. Rashidi et al. (2011) obtained the analytic approximate solutions for the radiative heat transfer of a micropolar fluid through a porous medium. Flow and heat transfer analysis of a viscoelastic fluid over a stretching sheet was addressed by Cortell (2006). Time-dependent three-dimensional flow of Maxwell fluid over a bidirectional stretching surface was examined by Awais et al. (2014). They have modeled the three-dimensional momentum equation for the unsteady flow of Maxwell fluid and resultant equations are solved analytically. Akbar et al. (2014a,b) addressed the MHD stagnation point flow due to shrinking of the sheet utilizing Carreau fluid. Later, this work has been extended to Prandtl fluid by Akbar et al. (2014a,b). Gireesha and Mahanthesh (2013) analyzed the flow and heat transfer of an unsteady Walters-B fluid through a porous medium with Hall effect and convective boundary condition. The heat and mass transfer flow of non-Newtonian Casson fluid under the influence of chemical reaction was discussed by Gireesha et al. (2015a,b) Gireesha et al. (2015c). Recently, Mahmood et al. (2015) reported an optimal solution for Oblique stagnation flow of Jeffery fluid toward a stretching surface.

Despite all the above mentioned non-Newtonian fluid models, the Eyring-Powell fluid model has two advantages. First, it is deduced from kinetic theory of liquid rather than the empirical relation as in the case of Power-law model. Secondly, it reduces to Newtonian behavior at low and high shear rates. Keeping this in view, Hayat et al. (2012a) Hayat et al. (2012b) considered the Powell-Eyring fluid flow over a moving surface with convective boundary condition and constant free stream. Jalil et al. (2013) studied the boundary layer flow and heat transfer of Powell-Eyring fluid over a continuously moving permeable surface in a parallel free stream. The authors employed scaling group of transformations to transform the governing partial differential equations into ordinary differential equations and then same are solved numerically using the Keller-box method. Boundary layer flow of an Eyring-Powell model fluid due to a stretching cylinder with variable viscosity was analyzed by Malik et al. (2013). Later, the numerical solutions for free convection heat and mass transfer of MHD Eyring-Powell fluid through a porous medium were presented by Eldabe et al. (2012). Hayat et al. (2013) investigated the radiation effects on the three-dimensional boundary layer flow of an Eyring-Powell fluid over a linear stretching sheet in the presence magnetic field via Homotopy analysis method. Recently, Akbar et al. (2015) reported the numerical solution for boundary layer flow of Eyring-Powell fluid over a stretching surface in the presence of uniform magnetic field.

Additionally, nanofluid is a new kind of energy transport fluid; it is a suspension of nanoparticles and a base fluid. Ordinary heat transfer fluids cannot be used for cooling rate requirements, since they have lower thermal conductivity. By embedding nanoparticles into ordinary fluids, their thermal performance can be improved significantly. Such thermal nanofluids for heat transfer applications represent a class of its own difference from conventional colloids for other applications. Nanofluids have a wide range of applications such as engine cooling, solar water heating, cooling of electronics, cooling of transformer oil, improving diesel generator efficiency, cooling of heat exchanging devices, improving heat transfer efficiency of chillers, domestic refrigerator-freezers, cooling in machining, in nuclear reactor, defense, space and etc Saidur et al. (2011). Choi (1995) was the first to prove that embedding nanoparticles into the base fluid enhances the thermal behavior of base fluid. Later on, Buongiorno (2006) addressed a comprehensive survey of convective transport in nanofluids. Oztop and Abu-Nada (2008) investigated the influence of various nanoparticles on flow and heat transfer due to buoyancy forces in a partially heated enclosure. They found that the use of nanoparticles causes heat transfer enhancement in the base fluid and this enhancement is more pronounced at a low aspect ratio than at a high one. Nield and Kuznetsov (2009) examined the nanoparticles influence on natural convection flow past a vertical plate saturated by porous medium. They have employed Brownian motion and thermophoresis effects by means of Buongiorno nanofluid model. The effect of heat generation/absorption on stagnation point flow of nanofluid over a surface with convective boundary condition was studied by Alsaedi et al. (2012). Makinde and Aziz (2011) addressed the boundary layer flow of a nanofluid past a stretching sheet with a convective boundary condition. A thermal radiation effect on boundary layer flow of a nanofluid over a heated stretching sheet with an unsteady free stream condition was numerically investigated by Das et al. (2014). They found that the heat transfer rate at the surface increases in the presence of Brownian motion but reverse effect occurs for thermophoresis. Chamkha et al. (2011) analyzed the mixed convection flow of a nanofluid past a stretching surface in the presence of Brownian motion and thermophoresis effects. Gireesha et al. (2014) obtained the numerical solutions for nanoparticle effect on boundary layer flow and heat transfer of a dusty fluid over a non-isothermal stretching surface. The influence of aligned magnetic field and melting heat transfer on stagnation point flow of nanofluid due to stretching surface was addressed by Gireesha et al. (2015a,b) Gireesha et al. (2015c). Nadeem et al. (2014a),(Nadeem et al., 2014b) studied

Please cite this article in press as: Mahanthesh, B. et al., Unsteady three-dimensional MHD flow of a nano Eyring-Powell fluid past a convectively heated stretching sheet in the presence of thermal radiation, viscous dissipation and Joule heating. Journal of the Association of Arab Universities for Basic and Applied Sciences (2016), http://dx.doi.org/10.1016/j.jaubas.2016.05.004

the Oblique stagnation point flow and heat transfer of non-Newtonian fluid over stretching surface in the presence of nanoparticles. Later, Nadeem et al. (2015) discussed the nanoparticle effect on Micropolar fluid flow between two horizontal plates. The influence of magnetic field and rotation effects are taken into consideration for the formulation. The peristaltic analysis of Eyring-Powell fluid in the presence of nanoparticles is carried out by Akbar (2015). Aforementioned studies on nanofluid are only concerned with two-dimensional flow situations. Only few attempts have been made to study three dimensional flow utilizing nanofluids (see Khan et al., 2014a,b; Mansur et al., 2014; Farooq and Hang, 2014; Hayat et al., 2015; Nadeem et al., 2014a,b; Gireesha et al., 2015a) Gireesha et al. (2015b) Gireesha et al. (2015c). Moreover, the viscous dissipation and Joule heating effects in most of the preceding attempts are ignored.

So far, no investigation is made which illustrates the unsteady three-dimensional flow of an Eyring-Powell fluid in the presence of nanoparticles. Therefore, current investigation deals with unsteady three-dimensional magnetohydrodynamic (MHD) flow of a nano Eyring-Powell nanofluid over a convectively heated stretching surface in the presence of radiation, viscous dissipation and Joule heating. Combined effects of heat and mass transfer involving Brownian motion and thermophoresis are also accounted. The conversation of mass, momentum, energy and nanoparticle volume fraction results in the complete formulation of nonlinear mathematical problem. The nonlinear analysis has been carried out for the velocity, temperature and nanoparticle concentration profiles using fourth-fifth order Runge–Kutta–Fehlberg method. To the best of our knowledge, this study has not been considered by any authors.

2. Mathematical formulation

Consider an unsteady three-dimensional boundary layer flow of an electrically conducting Eyring-Powell fluid past a convectively heated stretching sheet in the presence of nanoparticles. The Cartesian coordinates (x, y, z) are chosen with the origin O and the sheet coincides with the plane at $z = 0$ and flow occupies the region $z > 0$ as shown in Fig. 1. By keeping the origin fixed, the sheet is stretched in two laterals x- and y-directions with the velocities respectively in the form;

$$u_w(x,t) = \frac{ax}{1-\alpha t} \text{ and } v_w(y,t) = \frac{by}{1-\alpha t} \tag{2.1}$$

where a and b are positive constants.

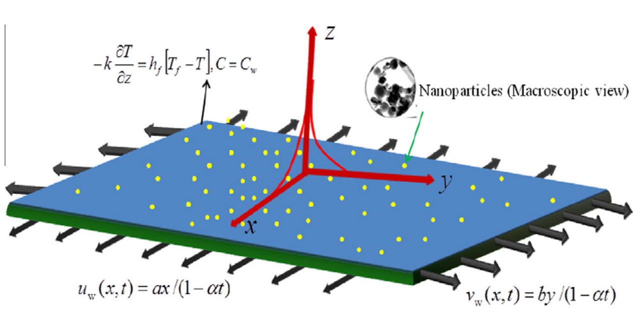

Figure 1 Physical model and coordinate system.

In polymer extrusion processes the material properties as well as elasticity of extruded sheet vary with time even though the sheet is pulled by constant force. It is also assumed that, T_f and C_w represents the convective temperature and concentration of nanoparticles at the sheet respectively, while T_∞ and C_∞ respectively denote the ambient fluid temperature and concentration. It is assumed that the Reynolds number is small so that an induced magnetic field is neglected. The applied transverse magnetic field is assumed to be variable kind and is considered in the special form as;

$$B = \frac{B_0}{(1-\alpha t)^{\frac{1}{2}}}. \tag{2.2}$$

The Cauchy stress tensor $\boldsymbol{T}$ for Eyring-Powell fluid can be given as

$$\mathbf{T} = -\mathbf{pI} + \tau \tag{2.3}$$

$$\rho_f \mathbf{a_i} = -\nabla p + \nabla.(\tau_{ij}) + \sigma \mathbf{J} \times \mathbf{B}, \tag{2.4}$$

here p is the pressure, $\boldsymbol{I}$ is identity tensor and τ_{ij} is extra stress tensor of Eyring-Powell fluid model, which is given as Hayat et al. (2013);

$$\tau_{ij} = \mu \frac{\partial u_i}{\partial x_j} + \frac{1}{\beta} \sinh^{-1}\left(\frac{1}{\gamma}\frac{\partial u_i}{\partial x_j}\right), \tag{2.5}$$

where β and γ are the characteristic length. By considering

$$\sinh^{-1}\left(\frac{1}{\gamma}\frac{\partial u_i}{\partial x_j}\right) \cong \frac{1}{\gamma}\frac{\partial u_i}{\partial x_j} - \frac{1}{6}\left(\frac{1}{\gamma}\frac{\partial u_i}{\partial x_j}\right)^3, \quad \left|\frac{1}{\gamma}\frac{\partial u_i}{\partial x_j}\right| < 1 \tag{2.6}$$

and using boundary layer approximations; the governing time-dependent three-dimensional equations for nano Eyring-Powell fluid are expressed in the presence of thermal radiation, viscous dissipation and Joule heating as Hayat et al. (2013);

$$\frac{\partial u}{\partial x} + \frac{\partial v}{\partial y} + \frac{\partial w}{\partial z} = 0, \tag{2.7}$$

$$\frac{\partial u}{\partial t} + u\frac{\partial u}{\partial x} + v\frac{\partial u}{\partial y} + w\frac{\partial u}{\partial z} = \nu\frac{\partial^2 u}{\partial z^2} + \frac{\mu}{\beta\gamma\rho_f^2}\frac{\partial^2 u}{\partial z^2} - \frac{1}{2\beta\gamma^3\rho_f}\left(\frac{\partial u}{\partial z}\right)^2\frac{\partial^2 u}{\partial z^2} - \frac{\sigma B^2}{\rho_f}u, \tag{2.8}$$

$$\frac{\partial v}{\partial t} + u\frac{\partial v}{\partial x} + v\frac{\partial v}{\partial y} + w\frac{\partial v}{\partial z} = \nu\frac{\partial^2 v}{\partial z^2} + \frac{\mu}{\beta\gamma\rho_f^2}\frac{\partial^2 v}{\partial z^2} - \frac{1}{2\beta\gamma^3\rho_f}\left(\frac{\partial v}{\partial z}\right)^2\frac{\partial^2 v}{\partial z^2} - \frac{\sigma B^2}{\rho_f}v, \tag{2.9}$$

$$\frac{\partial T}{\partial t} + u\frac{\partial T}{\partial x} + v\frac{\partial T}{\partial y} + w\frac{\partial T}{\partial z} = \alpha_m\frac{\partial^2 T}{\partial z^2} + \tau\left\{\mathrm{D_B}\left(\frac{\partial \mathrm{C}}{\partial \mathrm{z}}\frac{\partial \mathrm{T}}{\partial \mathrm{z}}\right) + \frac{\mathrm{D_T}}{\mathrm{T_\infty}}\left(\frac{\partial \mathrm{T}}{\partial \mathrm{z}}\right)^2\right\} - \frac{1}{\rho_f c_f}\frac{\partial q_r}{\partial z} + \frac{\mu}{\rho_f c_f}\left(\left(\frac{\partial u}{\partial z}\right)^2 + \left(\frac{\partial v}{\partial z}\right)^2\right) + \frac{\sigma B^2}{\rho_f c_f}(u^2 + v^2), \tag{2.10}$$

$$\frac{\partial C}{\partial t} + u\frac{\partial C}{\partial x} + v\frac{\partial C}{\partial y} + w\frac{\partial C}{\partial z} = \left[D_B\left(\frac{\partial^2 C D_T}{\partial z^2}\right) + \frac{D_T}{T_\infty}\frac{\partial^2 T}{\partial z^2}\right], \tag{2.11}$$

where u, v and w are velocity components along x, y and z directions respectively, T and C are temperature and volume fraction of nanoparticles respectively, ν – kinematic viscosity,

μ – dynamic viscosity, σ-electrical conductivity, $\alpha_m = k/\rho_f c_f$ – thermal diffusivity of the fluid, k – thermal conductivity of the fluid, D_B – Brownian diffusion coefficient, D_T – thermophoretic diffusion coefficient, $\tau = (\rho c)_p/(\rho c)_f$ – ratio of the effective heat capacity of nanoparticle and the heat capacity of ordinary fluid and t is the time.

Following Rosseland approximation, the radiative heat flux q_r is given by;

$$q_r = -\frac{4\sigma^*}{3k_1}\frac{\partial T^4}{\partial z}, \tag{2.12}$$

where σ^* – Stefan–Boltzmann constant and k_1 – mean absorption coefficient. In this model, optically thick radiation is considered. Assuming that the differences in temperature within the flow are sufficiently small such that T^4 can be expressed as a linear combination of the temperature about T_∞ as follows;

$$T^4 = T_\infty^4 + 4T_\infty^3(T - T_\infty) + 6T_\infty^2(T - T_\infty)^2 + \cdots \tag{2.13}$$

Now by neglecting higher order terms beyond the first degree in $(T - T_\infty)$, one can get

$$T^4 = 4T_\infty^3 T - 3T_\infty^4, \tag{2.14}$$

Using Eq. (2.14), the Eq. (2.12) takes the following form

$$\frac{\partial q_r}{\partial z} = -\frac{16\sigma^* T_\infty^3}{3k_1}\frac{\partial^2 T}{\partial z^2}, \tag{2.15}$$

Therefore using (2.15), the energy Eq. (2.10) becomes;

$$\frac{\partial T}{\partial t} + u\frac{\partial T}{\partial x} + v\frac{\partial T}{\partial y} + w\frac{\partial T}{\partial z} = \alpha_m\frac{\partial^2 T}{\partial z^2} + \tau\left\{D_B\left(\frac{\partial C}{\partial z}\frac{\partial T}{\partial z}\right) + \frac{D_T}{T_\infty}\left(\frac{\partial T}{\partial z}\right)^2\right\} + \frac{16\sigma T_\infty^3}{3\rho_f c_f k_1}\frac{\partial^2 T}{\partial z^2} + \frac{\mu}{\rho_f c_f}\left(\left(\frac{\partial u}{\partial z}\right)^2 + \left(\frac{\partial v}{\partial z}\right)^2\right) + \frac{\sigma B^2}{\rho_f c_f}(u^2 + v^2). \tag{2.16}$$

The relevant boundary conditions for the present problem are:

$$u = u_w(x,t),\ v = v_w(y,t),\ w = 0,\ k\frac{\partial T}{\partial z} = h_f(T - T_f),$$
$$C = C_w \text{at } z = 0,$$
$$U \to 0,\ v \to 0,\ \frac{\partial u}{\partial z} \to 0,\ \frac{\partial v}{\partial z} \to 0,\ T \to T_\infty,\ C \to C_\infty \text{ as } z \to \infty. \tag{2.17}$$

The Eqs. (2.7), (2.8), (2.9), (2.11) and (2.16) subject to the boundary conditions (2.17) admit similarity solutions in terms of the similarity functions f, g, θ, ϕ and the similarity variable η are defined as;

$$u = \frac{ax}{(1-\alpha t)}f'(\eta),\ v = \frac{by}{(1-\alpha t)}g'(\eta),$$
$$w = -\sqrt{\frac{v_f a}{(1-\alpha t)}}(f(\eta) + g(\eta)),\ \theta(\eta) = \frac{T - T_\infty}{T_f - T_\infty}, \tag{2.18}$$
$$\phi(\eta) = \frac{C - C_\infty}{C_w - C_\infty},\ \eta = \sqrt{\frac{a}{v_f(1-\alpha t)}}z.$$

In view of the Eq. (2.18), the continuity Eq. (2.7) is automatically satisfied and the remaining equations are reduced to the following set of non-linear ordinary differential equations;

$$(1+\varepsilon)f''' + (f+g)f'' - (f')^2 - S\left(f' + \frac{1}{2}\eta f''\right) - \varepsilon\delta_1(f'')^2 f''' - M^2 f' = 0, \tag{2.19}$$

$$(1+\varepsilon)g''' + (f+g)g'' - (g')^2 - S\left(g' + \tfrac{1}{2}\eta g''\right) - \varepsilon\delta_2(g'')^2 g''' - M^2 g' = 0, \tag{2.20}$$

$$\left(\frac{3+4R}{3Pr}\right)\theta'' + (f+g)\theta' - \frac{S}{2}\eta\theta' + Nb\phi'\theta' + Nt\theta'^2 + Ec_x f''^2 + Ec_y g''^2 + M^2 Ec_x f'^2 + M^2 Ec_y g'^2 = 0, \tag{2.21}$$

$$\frac{1}{Le}\phi'' + (f+g)\phi' - \frac{S}{2}\eta\phi' + \frac{N_t}{NbLe}\theta'' = 0. \tag{2.22}$$

The corresponding boundary conditions become;

$$f = 0,\quad g = 0,\quad f' = 1,\quad g' = c,$$
$$\theta' = Bi(\theta - 1),\quad \phi = 1,\quad \text{at } \eta = 0$$
$$f' \to 0,\ g' \to 0,\ f'' \to 0,\ g'' \to 0,\ \phi \to 0,\ \theta \to 0 \text{ as } \eta \to \infty, \tag{2.23}$$

where δ_1, δ_2 and ε are Eyring-Powel fluid parameters, c, M^2, S, Pr, Nb, Nt, R, Ec_x, Ec_y, Bi and Le are stretching ratio parameter, magnetic parameter, unsteady parameter, Prandtl number, Brownian motion parameter, thermophoresis parameter, thermal radiation parameter, Eckert number along x direction, Eckert number along y direction, Biot's number and Lewis number correspondingly. These parameters are defined as;

$$\delta_1 = \frac{u_w^3}{2vxC^2},\ \delta_2 = \frac{v_w^3}{2vyC^2},\ \varepsilon = \frac{1}{\mu\beta C},\ c = \frac{b}{a},\ Le = \frac{v}{D_B},$$
$$M^2 = \frac{\sigma B_0^2}{\rho_f a},\ S = \frac{\alpha}{a},\ Pr = \frac{v}{\alpha_m},\ Nb = \frac{\tau D_B(C_w - C_\infty)}{v},\ Bi = \frac{h_f}{k\sqrt{v/a}}, \tag{2.24}$$
$$Nt = \frac{\tau D_T(T_f - T_\infty)}{T_\infty v},\ R = \frac{4\sigma^* T_\infty^3}{\rho_f c_f \alpha_m k_1},\ Ec_x = \frac{u_w^2}{c_p(T_f - T_\infty)},$$
$$Ec_y = \frac{v_w^2}{c_p(T_f - T_\infty)}.$$

It is worthy to mention that, for $\varepsilon = \delta_1 = \delta_2 = 0$, the present problem reduces to Newtonian nanofluid problem and if $Nb = Nt = 0$ in Eq. (2.21), then it reduces to classical boundary layer heat equation.

2.1. Solution for particular case

Look at, for $c = 0$, the two dimensional case can be recovered. The Eq. (2.19) associated its boundary conditions with $\delta_1 = S = 0$ takes the following form

$$(1+\varepsilon)f''' + ff'' - (f')^2 - M^2 f' = 0, \tag{2.25}$$

$$f'(0) = 1,\ f(0) = 0,\ f'(\infty) = 0. \tag{2.26}$$

The exact solution of the Eq. (2.25) with respect to (2.26) is given by Hayat et al. (2013);

$$f(\eta) = \frac{1 - e^{-\xi\eta}}{\xi}, \ \xi = \sqrt{\frac{1 + M^2}{1 + \varepsilon}}. \tag{2.27}$$

The physical quantities of interest of nanofluid problems are local Nusselt number Nu or wall heat transfer and the local Sherwood number Sh or volume fraction mass transfer are defined as follows;

$$Nu = \frac{xq_w}{k(T_f - T_\infty)} \text{ and } Sh = \frac{xj_w}{D_B(C_w - C_\infty)}. \tag{2.28}$$

where q_w and j_w are the surface heat flux and surface mass flux respectively. Using similarity variables, we obtain

$$\frac{Nu}{\sqrt{Re_x}} = -\left(1 + \frac{4}{3}R\right)\theta'(0), \ \frac{Sh}{\sqrt{Re_x}} = -\phi'(0), \tag{2.29}$$

where $Re_x = u_w x/v$ is the local Reynolds number.

3. Method of solution and validation

The set of Eqs. (2.19)–(2.23) are highly nonlinear and coupled in nature, thus they are not amenable to closed form solutions. Therefore, they are solved numerically using a shooting technique coupled with fourth-fifth order Runge–Kutta–Fehlberg scheme with the help of algebraic software Maple. First, the non-linear boundary value problem has been reduced to system of linear differential equations by setting

$$f_1' = f_2,$$

$$f_2' = f_3,$$

$$(1 + \varepsilon - \varepsilon\delta_1 f_3^2)f_3' = -(f_1 + f_4)f_3 + f_2^2 + S(f_2 + 0.5\eta f_3) + M^2 f_2,$$

$$f_4 = g,$$

$$f_4' = f_5,$$

$$f_5' = f_6,$$

$$(1 + \varepsilon - \varepsilon\delta_2 f_6^2)f_6' = -(f_1 + f_4)f_6 + f_5^2 + S(f_5 + 0.5\eta f_6) + M^2 f_5,$$

$$f_7' = f_8,$$

$$\left(\frac{3 + 4R}{3Pr}\right)f_8' = -(f_1 + f_4)f_8 + 0.5S\eta f_8 - (Nbf_8 f_{10} + Ntf_8^2 + Ec_x f_3^2 + Ec_y f_6^2 + M^2 Ec_x f_2^2 + M^2 Ec_y f_5^2),$$

$$f_9' = f_{10},$$

$$\left(\frac{1}{Le}\right)f_{10}' = -(f_1 + f_4)f_{10} + 0.5S\eta f_{10} - \frac{Nt}{NbLe}f_8',$$

and relevant to the initial conditions are

$$f_1 = 0, f_2 = 1, f_3 = m_1, f_4 = 0, f_5 = c,$$

$$f_6 = m_2, f_7 = m_3, f_8 = Bi(m_3 - 1), f_9 = 1, f_{10} = m_4,$$

where unknown initial conditions m_1, m_2, m_3 and m_4 are calculated using iterative method called shooting method. The Shooting method is based on Maple implementation ‘shoot’ algorithm and is proven to be precise and accurate and which has been successfully used to solve wide range of non-linear problems in transport phenomena especially flow and heat transfer problems. A brief explanation of shooting method on maple implementation can be found in Meade et al. (1996). Then the resultant initial value problem has been solved using Runge–Kutta–Fehlberg fourth-fifth order method. The formula of RKF-45 method is given below;

$$\overline{y_{m+1}} = \overline{y_m} + h\left(\frac{25}{216}k_0 + \frac{1408}{2565}k_2 + \frac{2197}{4109}k_3 - \frac{1}{5}k_4\right), \tag{3.1}$$

$$\overline{y_{m+1}} = \overline{y_m} + h\left(\frac{16}{135}k_0 + \frac{6656}{12825}k_2 + \frac{28561}{56430}k_3 - \frac{9}{50}k_4 + \frac{2}{55}k_5\right), \tag{3.2}$$

$$k_0 = f(\overline{x_m}, \overline{y_m}),$$

$$k_1 = f\left(\overline{x_m} + \frac{h}{4}, \overline{y_m} + \frac{hk_0}{4}\right),$$

$$k_2 = f\left(\overline{x_m} + \frac{3}{8}h, \overline{y_m} + \left(\frac{3}{32}k_0 + \frac{9}{32}k_1\right)h\right),$$

$$k_3 = f\left(\overline{x_m} + \frac{12}{13}h, \overline{y_m} + \left(\frac{1932}{2197}k_0 - \frac{7200}{2197}k_1 + \frac{7296}{2197}k_2\right)h\right),$$

$$k_4 = f\left(\overline{x_m} + h, \overline{y_m} + \left(\frac{439}{216}k_0 - 8k_1 + \frac{3860}{513}k_2 - \frac{845}{4104}k_3\right)h\right),$$

$$k_5 = f\left(\overline{x_m} + \frac{h}{2}, \overline{y_m} + \left(-\frac{8}{27}k_0 + 2k_1 - \frac{3544}{2565}k_2 + \frac{1859}{4104}k_3 - \frac{11}{40}k_4\right)h\right),$$

where (3.1) and (3.2) are fourth and fifth order Runge–Kutta respectively. The inner iteration is counted until nonlinear solution converges with a convergence criterion of 10^{-6}. In addition, the step size is chosen as $\Delta\eta = 0.001$. In this scheme, it is most important to choose the appropriate finite values of η_∞. In accordance with standard practice in the boundary layer analysis the asymptotic boundary conditions at η_∞ are replaced by η_6.

The accuracy and robustness of the present method have been repeatedly confirmed in our previous publications (Gireesha et al., 2014). As a further check, the numerical results of $-\theta'(0)$ for different values of Nt and Nb are compared with that of Makinde and Aziz (2011) and Khan et al. (2015) for Newtonian fluid in the absence of viscous dissipation and Joule heating with $S = 0$, $Bi = 0.1$, $Le = Pr = 10$ and $c = 0$ in Table 1. This table shows that, comparison results are found to be an excellent agreement.

4. Result and discussion

In this section, the influence of various physical parameters like Eyring-Powell fluid parameters ($\varepsilon, \delta_1 \& \delta_2$), magnetic parameter ($M^2$), thermophoretic parameter (Nt), Brownian motion parameter (Nb), radiation parameter (R), Eckert numbers ($Ec_x \& Ec_y$) and Lewis number (Le) on axial velocity, transverse velocity, temperature and nanoparticles concentration profiles have been analyzed. Figs. 2–12 represent the velocity, temperature and the nanoparticle volume fraction profiles; and these profiles satisfy the far field boundary conditions (2.23) asymptotically, which also support the accuracy of the obtained numerical results. Table 2 presents the numerical

Table 1 Comparison of computed numerical values of $-\theta'(0)$ for different values of Nb and Nt with that of Makinde et al. (2011) and Khan et al. (2015) for $c=0, Le=Pr=10, Ec_x=Ec_y=R=0$ and $Bi=0.1$.

Nt	Makinde et al. (2011) $-\theta'(0)$		Khan et al. (2015) $-\theta'(0)$		Present study $-\theta'(0)$	
	$Nb=0.1$	$Nb=0.5$	$Nb=0.1$	$Nb=0.5$	$Nb=0.1$	$Nb=0.5$
0.1	0.092907	0.038325	0.0929	0.0383	0.092906	0.038324
0.2	0.092732	0.032498	0.0927	0.0324	0.092731	0.032497
0.3	0.092545	0.026905	0.0925	0.0269	0.092545	0.026905
0.4	0.092344	0.022010	0.0923	0.0220	0.092343	0.022010
0.5	0.092126	0.018035	0.0921	0.0180	0.092126	0.018034

Table 2 Numerical values of the Nusselt number $Re_x^{-1/2}Nu$ and the Sherwood number $Re_x^{-1/2}Sh$ for different values of $M^2, S, \varepsilon, Bi, R, Nb, Nt, Le, Ec_x$ and Ec_y for $Pr=3$.

M^2	S	ε	Bi	R	Nb	Nt	Le	Ec_x	Ec_y	$Re_x^{-1/2}Sh$	$Re_x^{-1/2}Sh$
0	0.4	0.5	0.4	1	0.5	0.5	1	0.2	0.2	0.401644	0.56512
0.5										0.278471	0.54910
1										0.152099	0.55200
0.5	0									0.376764	0.72948
	0.2									0.337336	0.64917
	0.3									0.311964	0.6008
0.5	0.4	0.6								0.291329	0.55841
		1.2								0.343583	0.6089
		1.8								0.373254	0.64659
0.5	0.4	0.5	0.01							0.01284	0.6332
			0.2							0.182807	0.57900
			0.6							0.336382	0.53098
0.5	0.4	0.5	0.4	0						0.095648	0.5942
				0.3						0.269923	0.56283
				0.6						0.212403	0.55152
0.5	0.4	0.5	0.4	1	0.2					0.340603	0.39862
					0.6					0.25685	0.56613
					1					0.16747	0.60087
0.5	0.4	0.5	0.4	1	0.5	0.2				0.302334	0.57877
						0.6				0.269973	0.54248
						1				0.232686	0.5365
0.5	0.4	0.5	0.4	1	0.5	0.5	0.5			0.307365	0.31006
							1.5			0.257914	0.78164
							2			0.244736	0.98679
0.5	0.4	0.5	0.4	1	0.5	0.5	0.5	0		0.459871	0.4652
								0.3		0.184582	0.59219
								0.6		0.10338	0.72669
0.5	0.4	0.5	0.4	1	0.5	0.5	0.5	0.2	0	0.341473	0.52025
									0.3	0.246696	0.56366
									0.6	0.108252	0.60792

values of Nusselt number and Sherwood number with respect to the variation of different parameters. It is observed that the Nusselt number increases with ε and Bi, but decreases qualitatively with an increase in M^2, S, Nb, Nt, Le, Ec_x and Ec_y. However, the Sherwood number is an increasing function of ε, Le, Nb, Ec_x and Ec_y, whereas this trend is quite opposite for S, Bi, R and Nt. Further it is observe that, the rate of heat and mass transfer for unsteady flow case ($S \neq 0$) is smaller as compared with steady flow case ($S=0$).

Fig. 2 depicts the primary and secondary velocity fields in steady and unsteady flow situations. The velocities are smaller for unsteady flow situation when compared to steady flow situation as shown in Fig. 2. It is also noted that, the velocity of Eyring-Powell fluid is larger than that of Newtonian fluid. Fig. 3 displays the temperature profile versus η for both steady and unsteady flow situations. It is observed that, the temperature field is higher for unsteady flow when compared to steady flow. Also, the temperature of nano-Newtonian fluid is higher than that of nano-Eyring-Powell, Newtonian and Eyring-Powell fluid in order. Fig. 4 portrays the effects of M^2&c on f'&g' distributions. It shows that an increase in M^2 leads to decrease f'&g' fields along with their corresponding boundary layer thickness. In fact the rate of transport decreases by increasing magnetic parameter, since the Lorentz force opposes the motion of fluid. It also reveals that by increasing stretching ratio parameter c, the velocity field f' decreases

Please cite this article in press as: Mahanthesh, B. et al., Unsteady three-dimensional MHD flow of a nano Eyring-Powell fluid past a convectively heated stretching sheet in the presence of thermal radiation, viscous dissipation and Joule heating. Journal of the Association of Arab Universities for Basic and Applied Sciences (2016), http://dx.doi.org/10.1016/j.jaubas.2016.05.004

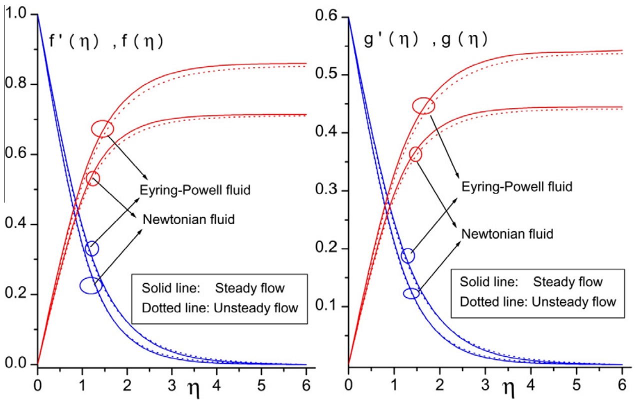

Figure 2 Variation of velocity distributions.

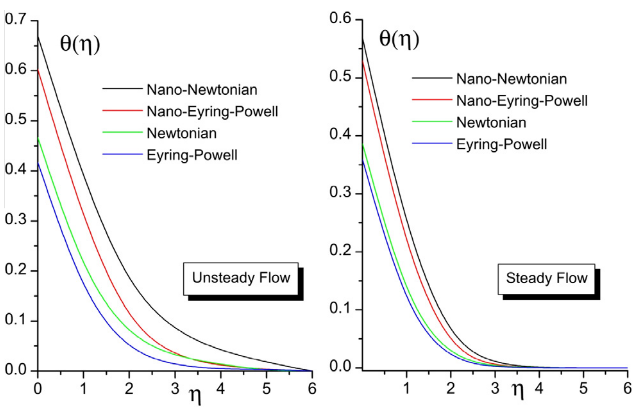

Figure 3 Variation of temperature distributions.

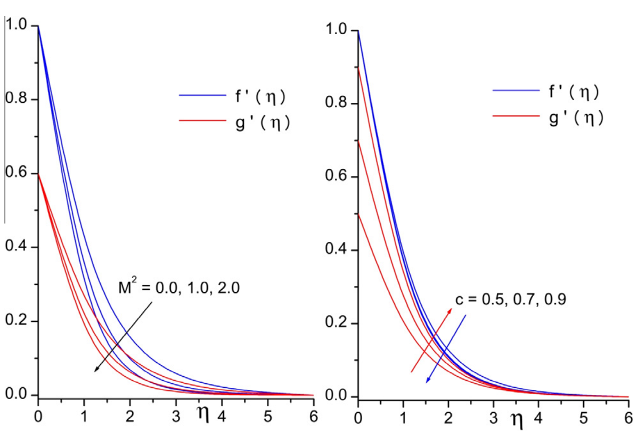

Figure 4 Effect of M^2&c on $f'(\eta)$ & $g'(\eta)$ profiles.

whereas opposite behavior is observed for g'. This is due to the fact that, the large values of $c(= b/a)$ lead to either increase in b or decrease in a. Consequently the velocity in x-direction decreases and velocity in y-direction increases respectively. This result is consistent with the results obtained by (Hayat et al., 2015).

Fig. 5 depicts f'&g' profiles for different values of ε&S. Analysis of this figure shows that by increasing ε the velocity fields f'&g' increases. Further, the f'&g' field's decreases ini-

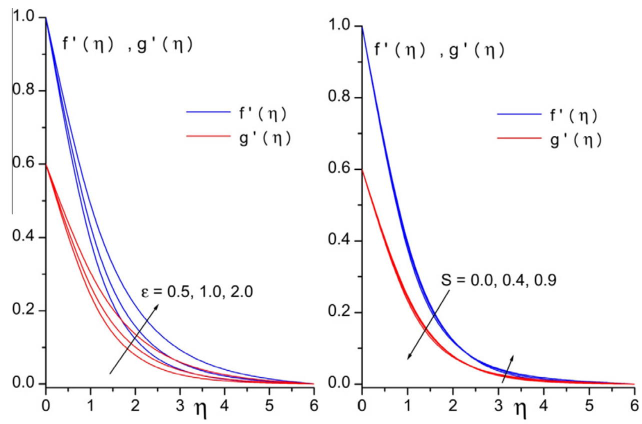

Figure 5 Effect of ε & S on $f'(\eta)$ & $g'(\eta)$ profiles.

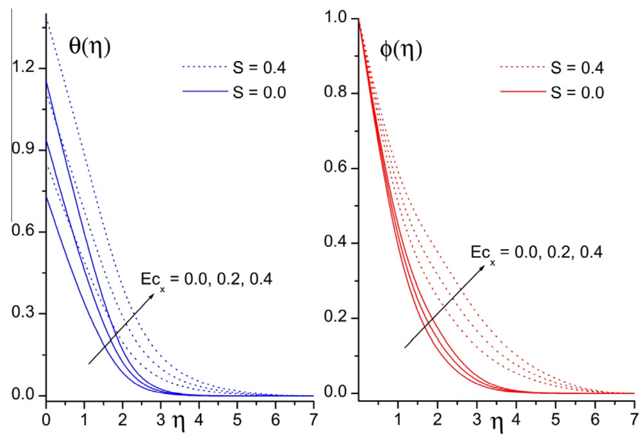

Figure 6 Effect of Ec_x on $\theta(\eta)$ & $\phi(\eta)$ profiles.

tially with S, but increase after a certain distance η from the sheet. The variation of Ec_x and Ec_y on temperature θ and nanoparticle volume fraction ϕ for steady and unsteady flow situations are respectively plotted in Figs. 6 and 7. These figures indicate that, θ and ϕ increases notably with an increase in Eckert number. Physically, by increasing the Eckert number, the heat energy is stored in the fluid due to the frictional or drag forces. As a result the fluid temperature field increases.

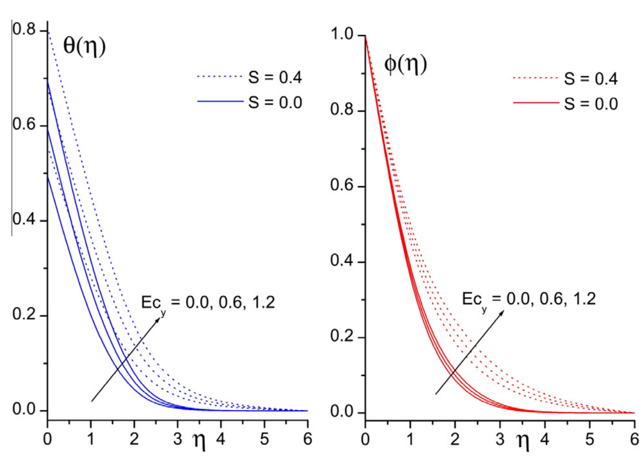

Figure 7 Effect of Ec_y on $\theta(\eta)$ & $\phi(\eta)$ profiles.

Please cite this article in press as: Mahanthesh, B. et al., Unsteady three-dimensional MHD flow of a nano Eyring-Powell fluid past a convectively heated stretching sheet in the presence of thermal radiation, viscous dissipation and Joule heating. Journal of the Association of Arab Universities for Basic and Applied Sciences (2016), http://dx.doi.org/10.1016/j.jaubas.2016.05.004

The Brownian motion and thermophoresis parameters appeared in both thermal and concentration boundary layer equation. It is worth to mentione that, $Nb\&Nt$ are coupled with the temperature and concentration field, and they play a tough role in determining the heat diffusion and concentration of nanoparticles in the boundary layer. We next move to analyze the effects of Nb and Nt on $\theta\&\phi$ profiles through the Figs. 8 and 9 respectively. It is observed that the temperature of the fluid increased considerably with an increase in Nb and Nt. On the other hand, the volume fraction of nanoparticle increase with an increase in Nt and an opposite trend has been observed as Nb varies. This is because, the random motion of nanoparticles get increased with an increase in Brownian motion parameter, which in turn an enhancement of fluid temperature and reduction of the nanoparticle diffusion.

Fig. 10 demonstrates the effect of unsteady parameter S on θ and ϕ profiles. It is observed that the temperature and nanoparticle concentration are augmented throughout the boundary layer region as S increases. It is due to the fact that S is inversely proportional to the stretching coefficient a. Thus an increase in S decreases the stretching rate. As a consequence the velocity decreases. This is responsible for an enhancement of temperature and nanoparticle volume fraction distributions in the boundary layer. We can also observe that θ and ϕ profiles are smaller for steady flow ($S = 0$) case in comparison with an unsteady flow ($S \neq 0$) case. Further, both θ and ϕ profiles are higher in the presence of viscous dissipation than in the absence.

The impact of Biot's number on temperature, and nanoparticle concentration is illustrated in Fig. 11. Physically, Biot's number is expressed as the convection at the surface of the body to the conduction within the surface of the body. When thermal gradient is applied on the surface, the ratio governing the temperature inside a body varies significantly, while the body heats or cools over a time. Normally, $Bi \ll 1$ represents uniform temperature field inside the surface, and $Bi \gg 1$ indicates the non-uniform temperature field inside the surface. From this plot it is observed that, temperature as well as nanoparticle concentration profiles monotonically increase with Biot's number. Finally, Fig. 12 illustrates the variation of $\theta\&\phi$ profiles within the boundary layer as R varies in both steady and unsteady flow situation. The temperature field as well as its corresponding thermal boundary layer thickness increased notably as R increases. Physically speaking, by strengthening radiation parameter provides more heat into the fluid, which leads to an intensification of the thermal boundary layer. It is also noted that, the effect of R is to decrease the nanoparticle volume fraction distribution near the stretching sheet, whereas reverse effect is observed far away from the sheet.

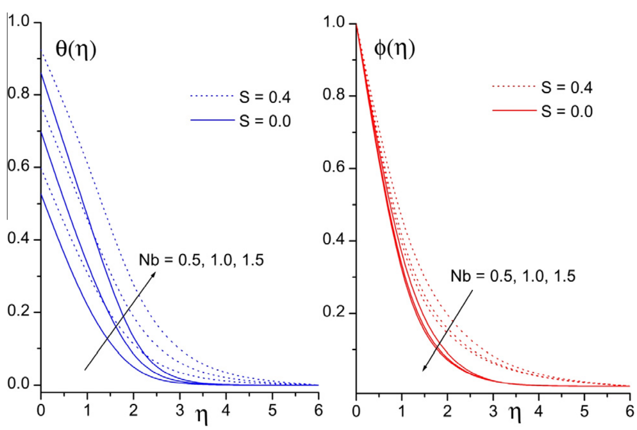

Figure 8 Effect of Nb on $\theta(\eta)$ & $\phi(\eta)$ profiles.

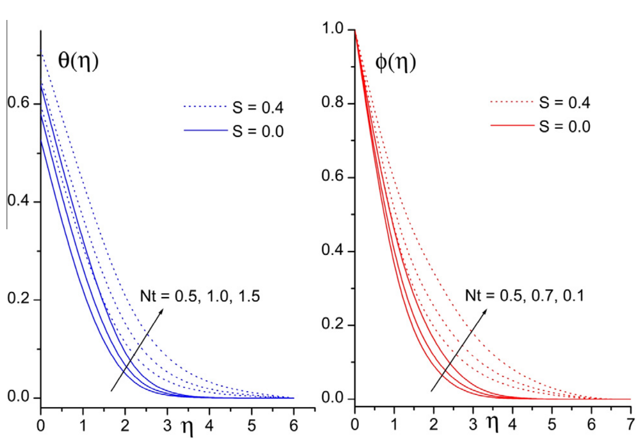

Figure 9 Effect of Nt on $\theta(\eta)$ & $\phi(\eta)$ profiles.

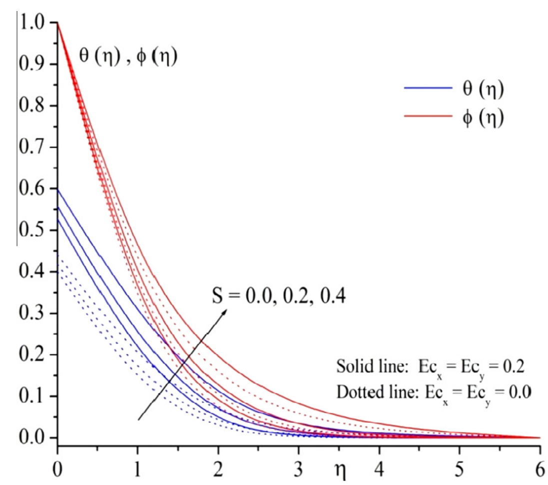

Figure 10 Effect of S on $\theta(\eta)$ & $\phi(\eta)$ profiles.

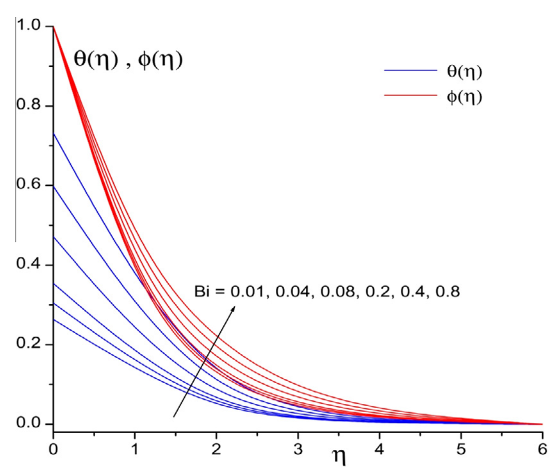

Figure 11 Effect of Bi on $\theta(\eta)$ & $\phi(\eta)$ profiles.

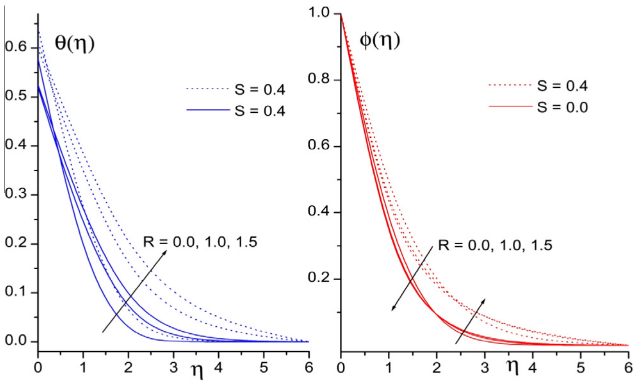

Figure 12 Effect of R on $\theta(\eta)$ & $\phi(\eta)$ profiles.

5. Concluding remarks

The problem of an unsteady 3-D boundary layer analysis of Eyring-Powell fluid over an impermeable linearly stretching sheet is studied in the presence of nanoparticles. A set of similarity transformation is presented to alter the boundary layer equations into self-similar form and then solved numerically. It is found that, the velocity field is larger for Eyring-Powel fluid than that of ordinary fluid. The influence of applied magnetic field reduces the velocity profile whereas opposite behavior is found for Eyring-Powell fluid parameter. The Brownian motion and thermophoresis mechanisms enhance the thermal behavior of the fluid. Further, an impact of viscous dissipation and thermal radiation plays a vital role in cooling and heating process. They should be kept minimum as much as possible in cooling systems.

Conflict of interest

The authors declare that there is no conflict of interest.

Nomenclature

a, b	constants	t	time (S)
c	stretching ratio parameter	T	fluid temperature (K)
B	magnetic field	$\boldsymbol{T}$	Cauchy stress tensor
B_0	magnetic field strength	T_f	surface temperature (K)
Bi	Biot number	T_∞	ambient Surface temperature (K)
C	nanoparticle volume fraction (kg/m^3)	u, v, w	velocity components along x, y and z directions (m s^{-1})
C_w	concentration at the wall (kg/m^3)	u_w, v_w	stretching sheet velocities along x, and y directions (m s^{-1})
C_∞	ambient nanofluid volume fraction (kg/m^3)	x, y, z	coordinates (m)
c_p	specific heat coefficient (J/kg K)		
D_B	Brownian diffusion coefficient	*Greek symbols*	
D_T	thermophoretic diffusion coefficient	θ	dimensionless temperature
Ec_x, $_{Ecy}$	Eckert numbers	ϕ	dimensionless nanoparticle volume fraction
f, g	dimensionless velocity fields	ν	kinematic viscosity of the fluid (m^2 s^{-1})
h_f	heat transfer coefficient	ε, δ_1, δ_2	Eyring-Powell fluid parameters
$\boldsymbol{I}$	identity Tensor	α_m	thermal diffusivity
$\boldsymbol{J}$	current Density	α	constant
j_w	nanoparticles mass flux	μ	dynamic viscosity (kg m^{-1} s^{-1})
k	thermal conductivity (W/m K)	β, γ	characteristics of Eyring-Powell fluid
k_1	mean absorption (W/m K)	σ	electric conductivity
Le	Lewis number	σ^*	Stefan–Boltzmann constant (W m^{-2} K^{-4})
M^2	magnetic parameter	η	similarity variable
Nb	Brownian motion parameter	τ	ratio of the effective heat capacity of the nanoparticle to that of an ordinary fluid
Nt	thermophoresis parameter	τ_{ij}	extra stress tensor of Eyring-Powell fluid
Nu	local Nusselt number	ρ	density (kg/m^3)
O	origin		
p	pressure	*Superscript*	
Pr	Prandtl number	$'$	derivative with respect to η
q_w	heat flux		
q_r	radiative heat flux (W m^{-2})	*Subscripts*	
R	thermal radiation parameter	f	fluid
Re_x	local Reynolds number	p	nanoparticles
S	unsteady parameter		
Sh	Sherwood number		

Acknowledgement

The author B.J. Gireesha gratefully acknowledges the financial support of UGC, New Delhi, India for pursuing this work under Raman Fellowship for Post Doctoral Research for Indian Scholars in USA 2014-2015.

References

Akbar, N.S., 2015. Application of Eyring-Powell fluid model in peristalsis with nano particles. J. Comput. Theor. Nanosci. 12, 94–100.

Akbar, N.S., Nadeem, S., Haq, R.U., Shiwei, Y., 2014a. MHD stagnation point flow of Carreau fluid towards a permeable shrinking sheet. Ain Shams Eng. J. 5, 1233–1239.

Akbar, N.S., Khan, Z.H., Haq, R.U., Nadeem, S., 2014b. Dual solutions in MHD stagnation-point flow of a Prandtl fluid impinging on a shrinking sheet. Appl. Math. Mech. 35, 813–820.
Akbar, N.S., Abdelhalim, E., Khan, Z.H., 2015. Numerical analysis of magnetic field on Eyring-Powell fluid flow towards a stretching sheet. J. Magn. Magn. Mater. 382, 355–358.
Alsaedi, A., Awais, M., Hayat, T., 2012. Effects of heat generation/absorption on stagnation point flow of nanofluid over a surface with convective boundary conditions. Commun. Nonlinear. Sci. Numer. Simul. 17, 4210–4223.
Awais, M., Hayat, T., Alsaedi, A., Asghar, S., 2014. Time-dependent three-dimensional boundary layer flow of a Maxwell fluid. Comput. Fluids 91, 21–27.
Buongiorno, J., 2006. Convective transport in nanofluids. ASME J. Heat Transfer 128, 240–250.
Chamkha, A.J., Gorla, R.S.R., Ghodeswar, K., 2011. Non-similar solution for natural convective boundary layer flow over a sphere embedded in a porous medium saturated with a nanofluid. Transp. Porous Media 86, 13–22.
Choi, S.U.S., 1995. Enhancing thermal conductivity of fluids with nanoparticles. ASME Fluids Eng. Div. 231, 99–105.
Cortell, R., 2006. A note on flow and heat transfer of a viscoelastic fluid over a stretching sheet. Int. J. Non-Linear Mech. 41, 78–85.
Crane, L.J., 1970. Flow past a stretching sheet. Z. Angew. Math. Phys 21, 645–647.
Das, K., Duari, P.R., Kundu, P.K., 2014. Nanofluid flow over an unsteady stretching surface in presence of thermal radiation. Alexandria Eng. J. 53, 737–745.
Eldabe, N.T.M., Sallam, S.N., Abou-zeid, M.Y., 2012. Numerical study of viscous dissipation effect on free convection heat and mass transfer of MHD non-Newtonian fluid flow through a porous medium. J. Egypt. Math. Soc. 20, 139–351.
Farooq, U., Hang, Xu, 2014. Free convection nanofluid flow in the stagnation-point region of a three-dimensional body. Sci. World J. 2014. Article ID 158269 14 pages.
Farooq, M., Rahima, M.T., Islamb, S., Siddiqui, A.M., 2013. Steady Poiseuille flow and heat transfer of couple stress fluids between two parallel inclined plates with variable viscosity. J. Assoc. Arab Univ. Basic Appl. Sci. 14, 9–18.
Gireesha, B.J., Mahanthesh, B., 2013. Perturbation solution for radiating viscoelastic fluid flow and heat transfer with convective boundary condition in nonuniform channel with Hall current and chemical reaction. ISRN Thermodyn., 14 Article ID 935481.
Gireesha, B.J., Mahanthesh, B., Gorla, R.S.R., 2014. Suspended particle effect on nanofluid boundary layer flow past a stretching surface. J. Nanofluids 3, 267–277.
Gireesha, B.J., Mahanthesh, B., Rashidi, M.M., 2015a. MHD boundary layer heat and mass transfer of a chemically reacting Casson fluid over a permeable stretching surface with non-uniform heat source/sink. Int. J. Ind. Math. 7, 14.
Gireesha, B.J., Mahanthesh, B., Shivakumara, I.S., Eshwarappa, K. M., 2015b. Melting heat transfer in boundary layer stagnation-point flow of nanofluid toward a stretching sheet with induced magnetic field. Eng. Sci. Technol. Int. J. http://dx.doi.org/10.1016/j.jestch.07.012.
Gireesha, B.J., Gorla, R.S.R., Mahanthesh, B., 2015c. Effect of suspended nanoparticles on three-dimensional MHD flow, heat and mass transfer of radiating Eyring-Powell fluid over a stretching sheet. J. Nanofluids 4, 1–11.
Gorla, R.S.R., Pop, I., Dakappagiri, V., 1995. Three-dimensional flow of a power-law fluid due to a stretching flat surface. ZAMM Z. Angew. Math. Mech. 75, 389–394.
Grubka, L.J., Bobba, K.M., 1985. Heat transfer characteristics of a continuous stretching surface with variable temperature. ASME J. Heat Transfer 107, 248–250.
Hayat, T., Naza, R., Asghar, S., Mesloub, S., 2012a. Soret-Dufour effects on three-dimensional flow of third grade fluid. Nucl. Eng. Des. 243, 1–14.
Hayat, T., Iqbal, Z., Qasim, M., Obaidat, S., 2012b. Steady flow of an Eyring Powell fluid over a moving surface with convective boundary conditions. Int. J. Heat Mass Transfer 55, 1817–1822.
Hayat, T., Awais, M., Asghar, S., 2013. Radiative effects in a three-dimensional flow of MHD Eyring-Powell fluid. J. Egypt Math. Soc. 21, 379–384.
Hayat, T., Muhammad, T., Shehzad, S.A., Alsaedi, A., 2015. Similarity solution to three dimensional boundary layer flow of second grade nanofluid past a stretching surface with thermal radiation and heat source/sink. AIP Adv. 5.
Ishak, A., Nazar, R., Pop, I., 2009. Boundary layer flow and heat transfer over an unsteady stretching vertical surface. Meccanica 44, 369–375.
Jalil, M., Asghar, S., Imran, S.M., 2013. Self similar solutions for the flow and heat transfer of Powell-Eyring fluid over a moving surface in a parallel free stream. Int. J. Heat Mass Transfer 65, 73–79.
Khan, J.A., Mustafa, M., Hayat, T., Farooq, M.A., Alsaedi, A., Liao, S.J., 2014a. On model for three-dimensional flow of nanofluid: an application to solar energy. J. Mol. Liq. 194, 41–47.
Khan, W.A., Khan, M., Malik, R., 2014b. Three-dimensional flow of an Oldroyd-B nanofluid towards stretching surface with heat generation/absorption. PLoS One 9.
Khan, J.A., Mustafa, M., Hayat, T., Alsaedi, A., 2015. Three-dimensional flow of nanofluid over a non-linearly stretching sheet: An application to solar energy. Int. J. Heat Mass Transfer 86, 158–164.
Mahmood, R., Nadeem, S., Akbar, N.S., 2015. Oblique stagnation flow of Jeffery fluid over a stretching convective surface: optimal solution. Int. J. Numer. Meth. Heat Fluid Flow 25, 454–471.
Makinde, O.D., Aziz, A., 2011. Boundary layer flow of a nanofluid past a stretching sheet with a convective boundary condition. Int. J. Therm. Sci. 50, 1326–1332.
Malik, M.Y., Hussain, A., Nadeem, S., 2013. Boundary layer flow of an Eyring-Powell model fluid due to a stretching cylinder with variable viscosity. Scientia Iranica 20 (2), 313–321.
Mansur, S., Ishak, A., Pop, I., 2014. Three-dimensional flow and heat transfer past a permeable exponentially stretching/shrinking sheet in a nanofluid. J. Appl. Math. 2014, 6.
Meade, D.B., Sharan, B., White, R.E., 1996. The shooting technique for the solution of two-point Boundary value problems. Maple Technol. 3, 85–93.
Nadeem, S., Rashidi, M., Akbar, N.S., 2014a. Oblique stagnation point flow of a Casson-Nano fluid towards a stretching surface with heat transfer. J. Comput. Theor. Nanosci. 11, 1422–1432.
Nadeem, S., Haq, R.U., Akbar, N.S., 2014b. MHD three-dimensional boundary layer flow of Casson nanofluid past a linearly stretching sheet with convective boundary condition. IEEE Trans. Nanotechnol. 13.
Nadeem, S., Masood, S., Rashid, M., Sadiq, M.A., 2015. Optimal and numerical solutions for an MHD micropolar nanofluid between rotating horizontal parallel plates. PLoS One. http://dx.doi.org/10.1371/journal.pone.0124016.
Nield, D.A., Kuznetsov, A.V., 2009. The Cheng-Minkowycz problem for natural convective boundary layer flow in a porous medium saturated by a nanofluid. Int. J. Heat Mass Transfer 52, 5792–5795.
Oztop, H.F., Abu-Nada, E., 2008. Numerical study of natural convection in partially heated rectangular enclosures filled with nanofluids. Int. J. Heat Fluid Flow 29, 1326–1336.
Rashidi, M.M., Mohimanianpour, S.A., Abbasbandy, S., 2011. Analytic approximate solutions for heat transfer of a micropolar fluid through a porous medium with radiation. Commun. Nonlinear Sci. Numer. Simul. 16, 1874–1889.
Saidur, R., Leong, K.Y., Mohammad, H.A., 2011. A review on applications and challenges of nanofluids. Renewable Sustainable Energy Rev. 15, 1646–1668.
Sakiadis, B.C., 1961. Boundary-layer behaviour on continuous solid surface. I. Boundary layer equations for two dimensional and axisymmetric flow. In: AIChE J. 7, 26–28.

Please cite this article in press as: Mahanthesh, B. et al., Unsteady three-dimensional MHD flow of a nano Eyring-Powell fluid past a convectively heated stretching sheet in the presence of thermal radiation, viscous dissipation and Joule heating. Journal of the Association of Arab Universities for Basic and Applied Sciences (2016), http://dx.doi.org/10.1016/j.jaubas.2016.05.004